Model of the local structure of random ternary alloys: Experiment versus theory

A. Balzarotti and N. Motta
Dipartimento di Fisica, Università degli Studi di Roma II, via Orazio Raimondo, I-00173 Roma, Italy

A. Kisiel and M. Zimnal-Starnawska
Institute of Physics, Jagiellonian University, Reymonta 4, PL-30-059, Cracow, Poland

M. T. Czyżyk
Theoretical Solid State Group of the General Physics Department, Institute of Physics, Jagiellonian University, Reymonta 4, PL-30-059 Cracow, Poland

M. Podgórny*
Institüt für Physik, Universität Dortmund, Postfach 500 500, D-4600 Dortmund 50, Germany
(Received 31 May 1984; revised manuscript received 26 December 1984)

We have performed an extended x-ray-absorption fine-structure (EXAFS) measurement of $Cd_{1-x}Mn_xTe$ solid solutions for various concentrations x in the single-phase range $0 \leq x \leq 0.7$. Data have been collected on the Mn K, Cd L_{III}, and Te L_{III} edges. We have found well-defined different nearest-neighbor Cd-Te and Mn-Te distances almost independent of x. A model of the microscopic structure of the zinc-blende-type $A_{1-x}B_xC$ ternary alloys based on a random distribution of cations has been developed. The model describes the bimodal distribution of near-neighbor distances in terms of distortion of the anion sublattice (the cation sublattice is assumed to remain fixed) with use only of the lattice constants of the alloy and the bond-stretching constants of each binary component. Its application to $Cd_{1-x}Mn_xTe$ and $In_{1-x}Ga_xAs$ alloys is proved to be in good agreement with the EXAFS results. Within the framework of this model we also consider the problem of the structural stability of $Cd_{1-x}Mn_xTe$.

I. INTRODUCTION

The CdTe-MnTe solid solutions, which combine the semiconducting properties of CdTe with the magnetic properties of the $3d^5$ states of Mn, have been recently studied with the main goal of providing a consistent explanation of their magnetic and electronic properties. Up to now, many significant results have been reported on this system concerning the optical,[1–4] magneto-optical,[5–7] transport,[8] and magnetic[9–12] properties throughout a wide range of Mn content. Nevertheless, there are still essential contradictions in the conclusions drawn from some investigations. In particular the photoluminescence studies[13] indicate that the d electrons of Mn are localized and placed about 1 eV below the top of the valence band. On the other band, the integral[14] and the angle-dependent[15] photoemission studies suggest a large delocalization and strong hybridization of the Mn $3d$ levels with the Te $5p$ valence band.

The atomic scale structure of the zinc-blende-type ternary alloys (like $Cd_{1-x}Mn_xTe$) is still an open question too. CdTe and MnTe crystallize in cubic (zinc-blende) and hexagonal (NiAs) structures, respectively. Standard x-ray diffraction measurements suggest that $Cd_{1-x}Mn_xTe$ crystallizes in the zinc-blende structure up to $x = 0.7$ and undergoes a structural phase transition to a multiple-phase system at higher concentrations of manganese.[16,17] The lattice constant of this material changes almost linearly with x in the whole single-phase region,[18] a feature commonly referred to as Vegard's law. Such behavior does not exclude a bimodal distribution of the nearest-neighbor (NN) distances in the alloy. Diffraction methods do not provide sufficient structural information on the interatomic distances in these crystals. A new insight was recently supplied by an extended x-ray-absorption fine-structure (EXAFS) analysis applied to the $In_{1-x}Ga_xAs$ alloys by Mikkelsen and Boyce,[19] and to the $Er_{1-x}Pr_xSb$ alloys by Azoulay *et al.*,[20] although in a very narrow range of composition x. These works, together with our experimental results reported earlier for $Cd_{1-x}Mn_xTe$,[21,22] yield the conclusion that impurity atoms create a bimodal distribution of the NN distances.

There was other experimental evidence which forced us to consider the NN and the NNN (next-nearest-neighbor) order in this alloy; for instance, the analysis of an anomalous behavior of the $Cd_{1-x}Mn_xTe$ fundamental reflectivity spectra at various Mn concentrations,[18,23,24] which might suggest that the Mn atoms induce local disorder, or the results of the investigation of the magnetic properties obtained by Gałazka *et al.*[10] Moreover, the recent calculation of the electronic states in hypothetical, cubic MnTe,[25] in which the lattice constant was extrapolated to $x = 1$ from the linear behavior in the homogeneity region, showed that, regardless of the assumed charge transfer, the resulting structure was metallic, in apparent contradiction with expectations. The improper structural information used there was perhaps a reason for this discrepancy. Therefore, definite structural information is

apparently needed to explain the electronic and magnetic properties of $Cd_{1-x}Mn_xTe$.

Our paper is devoted solely to that problem. In Sec. II we present the results of the EXAFS measurements performed on the binary compounds CdTe and MnTe and on their alloys, and discuss the NN distances between components. Next, in Sec. III, we develop a model of the microscopic structure of the zinc-blende-type $A_{1-x}B_xC$ ternary alloys which explains consistently the experimentally found bimodal distribution of NN distances. Section IV contains a summary of our experimental and theoretical results, a comment about the different approximations in the theory of alloys, and, finally, a discussion about the stability of $Cd_{1-x}Mn_xTe$ alloys.

II. EXPERIMENTAL DETAILS AND DATA REDUCTION

The EXAFS measurements were performed at the National Radiation Facility [Programma per l'utilizzazione della Luce di Sincrotrone (PULS)] of the Laboratori Nazionali di Frascati (Italy) with the light emitted by the ADONE storage ring (1.5 GeV, 50 mA). The experimental setup is described elsewhere.[26]

Single crystals of CdTe and MnTe and of their alloys were powdered and supported on Kapton and Mylar adhesive tape, or deposited from a water dispersion on Millipore membranes. For CdTe, thin films 2.6 μm thick evaporated on a mica substrate were also used. EXAFS spectra were measured at three different temperatures: 300, 150, and 80 K for Mn concentrations $x=0$, 0.1, 0.3, 0.5, 0.7, and 1. The edges considered were the Te L_{III} and L_I, the Cd L_{III} and L_I, and the Mn K at 4341, 4939, 3537, 4018, and 6543 eV, respectively. The Mn K edge was measured by fluorescence. In MnTe the steepest edge was at 6545 eV. The average resolution was better than 10^{-4} in this energy range. To check the homogeneity of our solid solutions in the whole composition range and to measure their lattice constant, we performed an x-ray diffraction study. In Fig. 1 we present the measured lattice constant as a function of the Mn fraction x. The x-ray results indicated that the alloys were not composed of separate CdTe and MnTe phases and that the average lattice constant varied almost linearly through the entire solid solution.

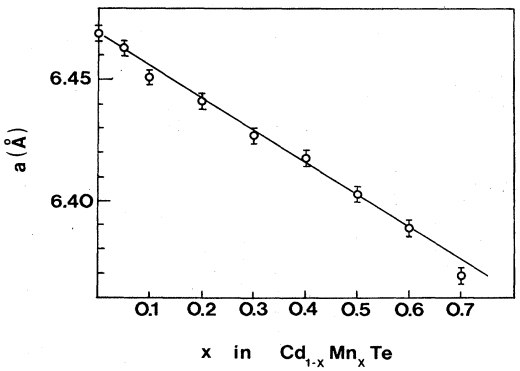

FIG. 1. Lattice constant of $Cd_{1-x}Mn_xTe$ vs Mn content x as measured by x-ray diffraction.

The extraction of the EXAFS modulation function $\chi(k)$ from the background was made with the usual procedure of data reduction, i.e., a Victoreen fit to subtract the pre-edge background followed by a spline line fit to the atomiclike smooth background. This procedure yields the well-known EXAFS function

$$\chi(k)=\sum_j N_j \frac{f_j(\pi,k)}{kR_j^2}\exp(-2R_j/\lambda)\exp(-2k^2\sigma_j^2) \times\sin[2kR_j+\phi_j(k)] , \quad (1)$$

where N_j is the coordination number of the jth shell at a distance R_j from the absorber, $f_j(\pi,k)$ is the backscattering amplitude for the jth atom, $\phi_j(k)$ is the total (backscatterer and absorber) phase shift, $\lambda(k)$ is the mean free path of the excited electron, and σ_j^2 is the mean-square relative displacement of the absorber-backscatterer pair. The photoelectron wave vector k is given by

$$\hbar\omega=E_0+\frac{\hbar^2k^2}{2m} , \quad (2)$$

where E_0, the photoabsorption threshold, has been taken to coincide with the maximum of the derivative at the absorption edge.

The total phase and backscattering amplitude for the jth shell were obtained from the usual analysis[27] in **k** space. Namely, the $k\chi(k)$ data were Fourier-transformed (FT) to real space and the contribution of the single shell j was backtransformed to extract the phase and amplitude functions. From Eq. (1) the total phase factor $\phi_j(k)$ for a given shell j contained in the sine function can be extracted if the interatomic distance is known, viz., a suitable structural standard can be found. In our case the zinc-blende CdTe and the hexagonal MnTe binary compounds were adopted. Under the assumption of the phase transferability for a given absorber-backscattered pair, i.e., $\phi_j^x(k)=\phi_j^M(k)$, and from the relation $\Phi_j^x(k)=2kR_j^x+\phi_j^x(k)$, the interatomic distance $R_j^x(k)$ for the unknown is simply given by

$$R_j^x(k)=[\Phi_j^x(k)-\phi_j^M(k)]/2k , \quad (3)$$

where M stands for model compound. Before discussing the ternary alloy data, we shall examine the EXAFS of the standards at their different edges.

A. CdTe

CdTe, similar to a large number of II-VI compounds, is a semiconductor which crystallizes in the zinc-blende structure. This structure is characterized by the tetrahedral coordination of atoms, i.e., each atom of Cd is surrounded by four NN Te atoms at the same distance. Cd ($Z=48$) and Te ($Z=52$) are neighbors in the Periodic Table and this implies that their backscattering functions should be rather similar. For intermediate-Z atoms this function exhibits a double peak due to the Ramsauer-Townsend effect.[27] As a result we expect a double peak in the modulus of $F(R)$, provided $\chi(k)$ is transformed on a sufficiently extended k range.

The Te L_{III}—edge EXAFS of CdTe is presented in Fig.

2 together with its FT calculated in the range $2.6 \leq k \leq 8.1$ Å^{-1} using a Hanning window function. The first peak is double and corresponds to the first Cd shell at $R = 2.80$ Å. The experimentally derived amplitude function $f(\pi,k)$ for this shell is given by

$$f(\pi,k) = \frac{A(k) R_{\mathrm{CdTe}}^2}{N_{\mathrm{Cd}} \exp[-2R_{\mathrm{CdTe}}/\lambda(k)] \exp(-2k^2\sigma_{\mathrm{CdTe}}^2)} . \quad (4)$$

The amplitude function $f(\pi,k)$ is plotted in Fig. 2(c) and displays a clear double maximum. The comparison with the theoretical amplitude function from the Teo-Lee tabulations[28] indicates that only rough agreement exists. Considerable work has been done on ZnSe and ZnTe by Stern *et al.*,[29] who based their analyses of the EXAFS spectra on the influence of many-body effects on the amplitude backscattering function. Fitting the spectra with the theoretical parameters and correcting for the electron-electron interaction through external S_0^2 and λ parameters, reasonable agreement with experiment was achieved. On the other hand, Pettifer[30] critically examined the EXAFS results for ZnSe and ZnTe and concluded that the agreement between theory and experiment was not satisfactory for shells other than the first. The main difficulty was found in the use of the plane-wave approximation for the backscattering functions. These functions differ strongly for heavier elements ($Z > 40$) at values of k lower than 8 Å^{-1} from those calculated within the spherical wave approximation. Contrary to Stern *et al.*,[29] Pettifer[30] suggests a significant effect on the NN back-

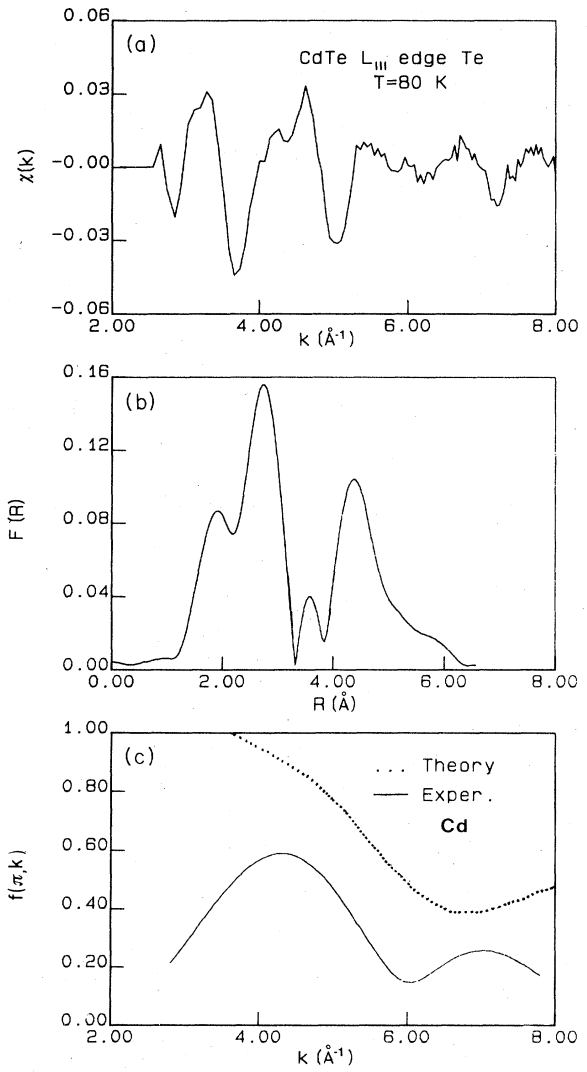

FIG. 2. (a) EXAFS modulation function $\chi(k)$ above the L_{III} edge of Te in CdTe. (b) Modulus $F(R)$ of the Fourier transform (FT) of $\chi(k)$ in the range $2.6 \leq k \leq 8.1$ Å^{-1} using a Hanning window function. (c) Comparison between the theoretical (dotted line) and experimental amplitude functions of Cd obtained by backtransforming the first two peaks of $F(R)$.

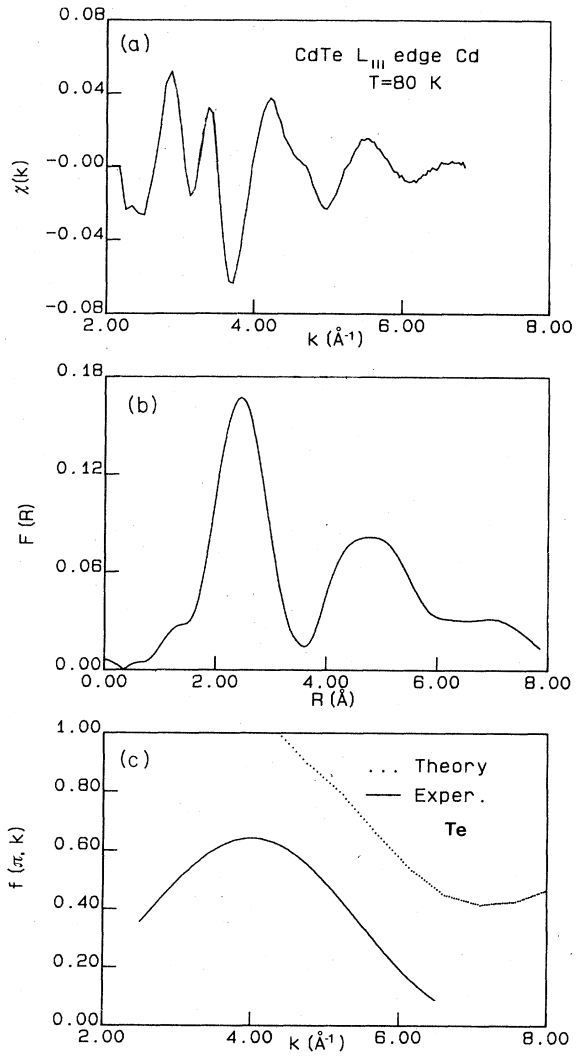

FIG. 3. (a) EXAFS modulation function $\chi(k)$ above the L_{III} edge of Cd in CdTe. (b) Modulus $F(R)$ of the FT of $\chi(k)$ in the range $2.0 \leq k \leq 6.7$ Å^{-1} using a Hanning window function. (c) Comparison between the theoretical (dotted line) and experimental amplitude functions of Te obtained by backtransforming the first peak of $F(R)$.

scattering of the curvature of the outgoing electron wave for all chalcogenide zinc compounds ZnS, ZnSe, and ZnTe.

A preliminary analysis of CdTe was made on the same lines of a previous study[21] where the main interest was on the corrections to be applied to Eq. (1). At the L_{III} edge of Cd, measured at 80 K, the NN Te shell is not resolved into two structures like it is at the Te L_{III} edge, because of the narrower range of k accessible to the measurements (Fig. 3). Furthermore, the amplitude function in Fig. 3(c) shows that the second peak occurs at values of k larger than 6 Å^{-1}. Although the identification of the main features of $F(R)$ can generally be made using only theoretical scattering functions,[21] the exact knowledge of these functions cannot be obtained. In view of these difficulties we treat CdTe as a standard from which these functions are experimentally derived and used in the analysis of the alloys.

B. MnTe

MnTe has a well-defined hexagonal crystallographic structure (NiAs-type lattice) in which Mn is sixfold coordinated to Te with a NN distance of 2.909 Å. Here we are interested in achieving experimental scattering functions for the Mn-Te and the Te-Mn pairs to build a model environment for the cubic $Cd_{1-x}Mn_xTe$ alloys, by using the concept of transferability of the scattering phase in the high-electron-kinetic-energy regime. We have measured, therefore, the EXAFS structures above the Mn K edge and the Te L_{III} edge in MnTe, which are shown in Figs. 4(a) and 5(a), respectively. The corresponding $F(R)$

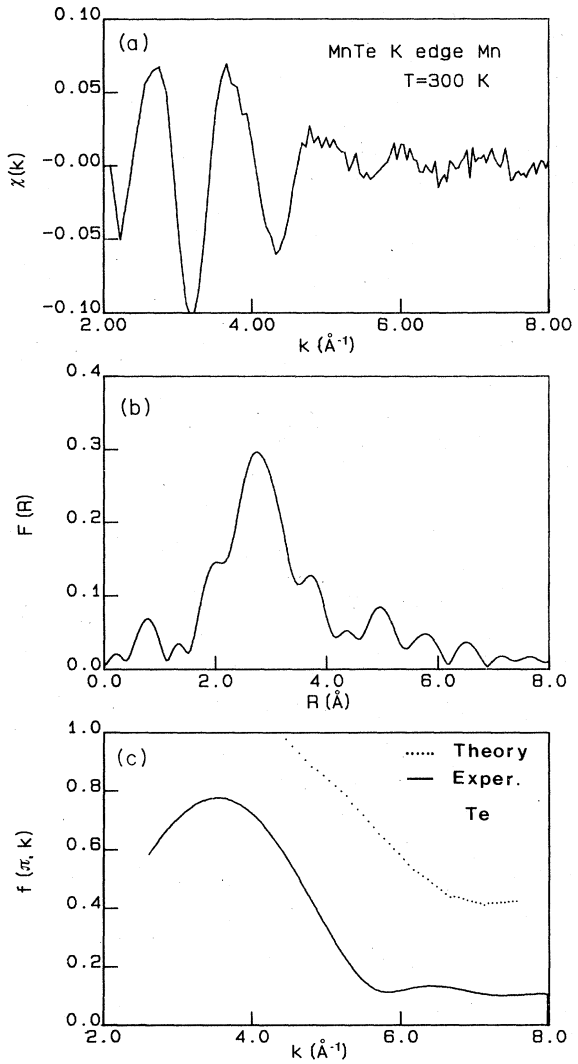

FIG. 4. (a) EXAFS modulation function $\chi(k)$ above the K edge of Mn in MnTe. (b) Modulus $F(R)$ of the FT of $\chi(k)$ in the range $2.1 \leq k \leq 8.5$ Å^{-1} using a Hanning window function. (c) Comparison between the theoretical (dotted line) and experimental amplitude functions of Te obtained by backtransforming the peak of $F(R)$ between 1.5 and 3.4 Å.

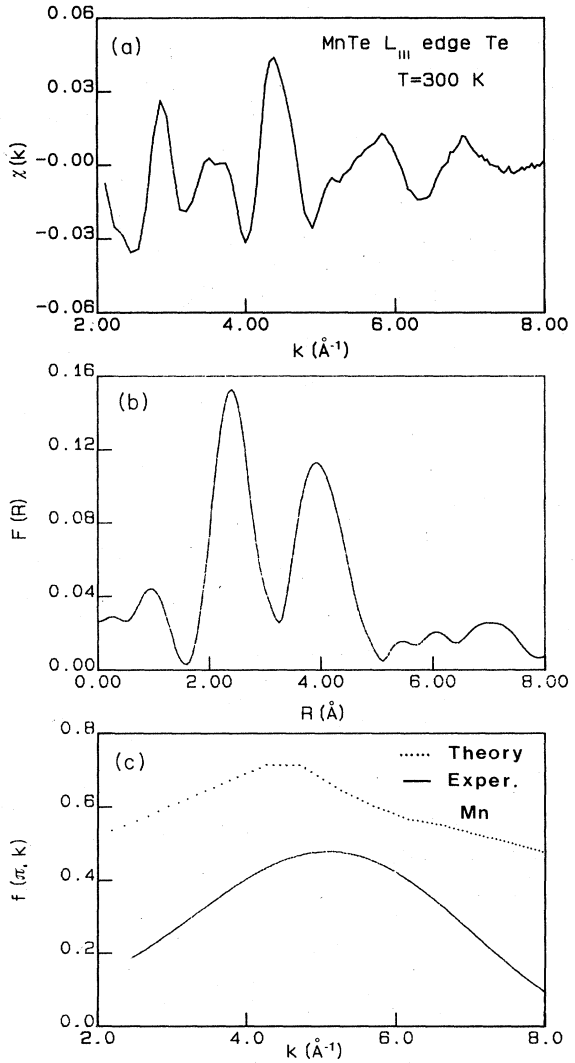

FIG. 5. EXAFS modulation function $\chi(k)$ above the L_{III} edge of Te in MnTe. (b) Modulus $F(R)$ of the FT of $\chi(k)$ in the range $2.1 \leq k \leq 8.5$ Å^{-1} using a Hanning window function. (c) Comparison between the theoretical (dotted line) and experimental amplitude functions of Mn obtained by backtransforming the first peak of $F(R)$.

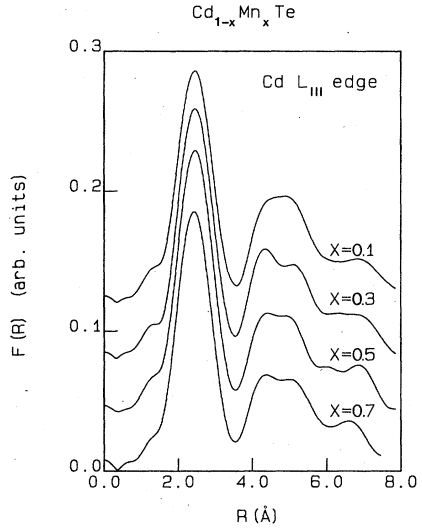

FIG. 6. Modulus $F(R)$ of the FT of $\chi(k)$ measured above the Cd L_{III} edge in $Cd_{1-x}Mn_xTe$ for several concentrations x.

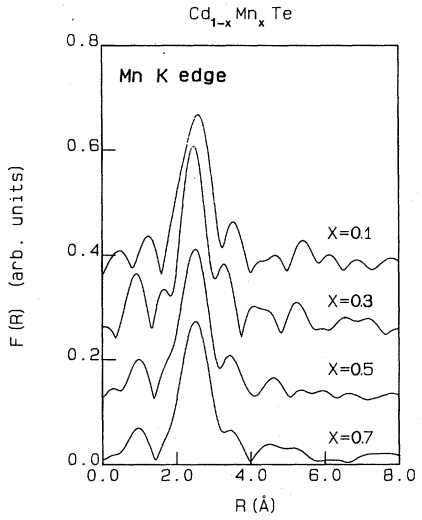

FIG. 8. Modulus $F(R)$ of the FT of $\chi(k)$ measured above the Mn K edge in $Cd_{1-x}Mn_xTe$ for several concentrations x.

are displayed in Figs. 4(b) and 5(b), respectively. In Figs. 4(c) and 5(c) we present the $f_j^M(\pi,k)$ functions extracted using the same procedure as described above. These functions are used subsequently to fit the $Cd_{1-x}Mn_xTe$ EXAFS data.

C. $Cd_{1-x}Mn_xTe$

1. *Cd L_{III} edge*

The $F(R)$ spectra around the Cd L_{III} edge for $x=0.1$, 0.3, 0.5, and 0.7 in $Cd_{1-x}Mn_xTe$ are illustrated in Fig. 6. Due to the limited k range accessible above this edge, free from the absorption of the L_{II} Cd edge, the achieved resolution in the **r** space is worse than around Te, and the double components of the first peak are not observed. Moreover, the width of the Te peak is approximately the same for the various concentrations of manganese. By filtering out the first peak of $F(R)$ and backtransforming it in the range $1.5 \leq R \leq 3.5$ Å, we obtained, from Eq. (3), the $R(k)$ values of the Cd-Te pair for various x values, which are shown in Fig. 7. Within the estimated error bar for this distance ($\simeq$0.01 Å), we measured a Cd-Te distance of 2.80 Å for all concentrations. Such a distance coincides with that of pure CdTe.

2. *Mn K edge*

The above analysis applied to the Mn K edge yields a distance of the Te-Mn pair ranging from 2.76±0.01 Å for $x=0.1$ to 2.74±0.01 Å for $x=0.7$. The measured $F(R)$ spectra are shown in Fig. 8 and the $R(k)$ function is plotted in Fig. 9 for various x values.

3. *Te L_{III} edge*

Figure 10(a) shows the $F(R)$ function above the Te L_{III} edge for x increasing from 0.1 to 0.7, calculated in the range $2.6 \leq k \leq 8.1$ Å. The first and second peaks of $F(R)$ correspond to the NN Mn and Cd atoms, respectively, in the first shell surrounding Te. By increasing

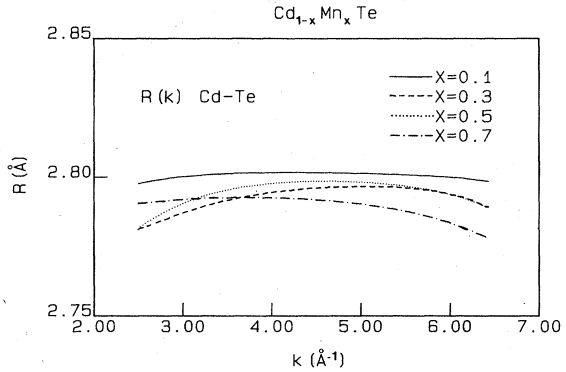

FIG. 7. Nearest-neighbor Cd-Te distances vs k as derived from the EXAFS analysis of $Cd_{1-x}Mn_xTe$ for several concentrations x.

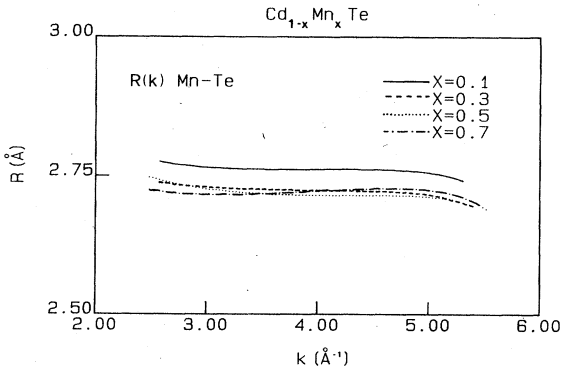

FIG. 9. Nearest-neighbor Mn-Te distances vs k as derived from the EXAFS analysis of $Cd_{1-x}Mn_xTe$ for several concentrations x.

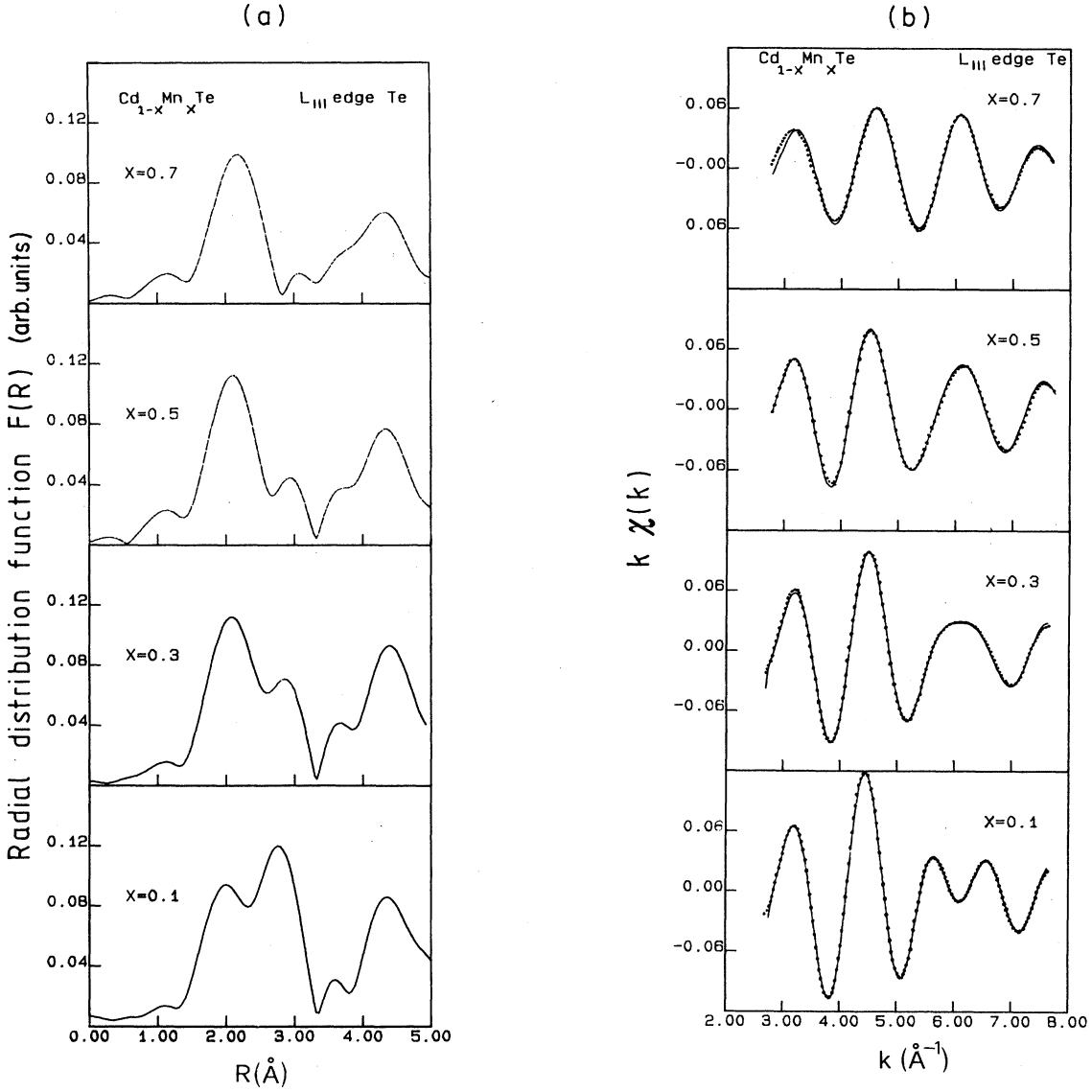

FIG. 10. (a) Modulus $F(R)$ of the FT of $\chi(k)$ at the L_{III} edge of Te for four Mn concentrations x in $Cd_{1-x}Mn_xTe$. (b) Back-Fourier transforms of the $F(R)$ curves of (a) in the region 1.3—3.3 Å (solid lines). The dotted curves represent the best fit to the NN Mn and Cd distributions around Te.

the mole fraction of Mn, the intensity of the Mn peak increases and, correspondingly, the intensity of the Cd peak decreases. As discussed in the case of pure CdTe, the Cd peak is double and thus the Mn peak in the alloy is superimposed on the lateral peak of Cd.

The back-Fourier-transforms $k\chi(k)$ obtained from the first two shells of $F(R)$ are shown in Fig. 10(b) (solid lines). We have best-fitted them by using as free parameters the anion-cation distances, the Debye-Waller factors, and the shifts of E_0 with respect to the model compounds

TABLE I. Best-fitted anion-cation distances R, Debye-Waller factors σ^2, and change of E_0 for the Mn-Te and Cd-Te pairs.

	Mn-Te			Cd-Te		
x	R (Å)	σ^2 (10^{-2} Å^2)	ΔE_0 (eV)	R (Å)	σ^2 (10^{-2} Å)	ΔE_0 (eV)
0.1	2.755	0.245	−0.556	2.801	0.620	0.333
0.3	2.751	0.229	0.250	2.801	0.592	1.050
0.5	2.747	0.250	0.377	2.800	0.650	2.568
0.7	2.737	0.720	2.090	2.798	1.800	6.620

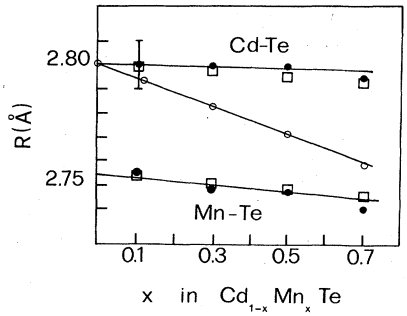

FIG. 11. Average Cd-Te and Mn-Te nearest-neighbor distances in $Cd_{1-x}Mn_xTe$ alloys vs concentration x. Solid circles are values from the best fit of the EXAFS data; open squares are values calculated from the model, and open circles are values of $a(x)\sqrt{3}/4$, as measured by x-ray diffraction.

(Table I). The starting values were those derived from the analysis of the Cd L_{III} and the Mn K edges in $Cd_{1-x}Mn_xTe$. The amplitude and phase functions were determined from the model compounds and the coordination numbers were calculated from the nominal concentration in the alloy. The best-fitted $k\chi(k)$ curves are reproduced in Fig. 10(b) (dotted lines) for various x values and agree satisfactorily with the experimental curves. The anion-cation distances are almost independent of x and are shown in Fig. 11 (solid dots). In $In_{1-x}Ga_xAs$ Mikkelsen and Boyce[19] could not directly observe the splitting of the cation peak. They observed, instead, a broadening and a small shift of the NN peak compared with the pure binary compounds. They resolved it by a fitting procedure using two Gaussian distributions.

In $Cd_{1-x}Mn_xTe$ the other peaks of $F(R)$ between 3 and 5 Å are assigned to the NNN Te and the Cd(Mn) atomic shells.

III. MODEL OF THE MICROSCOPIC STRUCTURE OF RANDOM ALLOYS

Taking into account all the experimental evidence, it seems that a general property of random solid solutions of binary compounds has been discovered: the A-C and B-C distances in the zinc-blende-type $A_{1-x}B_xC$ alloy at arbitrary concentration are nearly the same as in pure AC and BC compounds, respectively. It is therefore very interesting to consider in detail how the zinc-blende structure accommodates two different cation-anion distances. Mikkelsen and Boyce[19] drew an analogy between the $A_{0.5}B_{0.5}C$ alloy and the chalcopyrite (ABX_2) crystallographic structures. They did not, however, model the disordered phase and, following their approach directly, one cannot describe an alloy at arbitrary concentration x.

In order to develop a model possessing such a capability, one must realize that NN distances, as measured by EXAFS, are an average over a macroscopic volume. It is implied that a model must be statistical, and proper averaging over possible NN distances should reproduce the experimental data.

To start with, we shall consider which sublattice is more likely to be distorted. Our measurements do not provide enough information to analyze the NNN distances. Mikkelsen and Boyce[19] report that the cation-cation distribution has a single peak and is only slightly broadened compared to that in the pure compound, whereas the anion-anion distribution is bimodal. Such experimental evidence suggests that much stronger distortion occurs to the anion sublattice. Moreover, as Mikkelsen and Boyce[19] pointed out, if the cation sublattice were to distort, the average anion-cation distance could not differ much from the virtual-crystal-approximation (VCA) value. Decreasing the distance of a cation from some anion, we increase the other cation-anion distances in the same tetrahedron, keeping the average close to the VCA value. Finally, we point out that if we believe that the NN interactions are dominant in the alloy, it is very likely that the anion surrounded by different cations will leave its central position in the tetrahedron. The same process is not very likely to happen for the cation, always surrounded by four identical anions.

A. Formulation of the model

Taking into account the above considerations we construct our model of the microscopic structure of the zinc-blende-type $A_{1-x}B_xC$ alloy according to the following:

(i) We assume that the cation sublattice remains undistorted. (In the case of alloys containing two different anions the anion sublattice remains undistorted.)

(ii) We consider all the possible coordinations around an anion in the alloy—there can be 0, 1, 2, 3, and 4 B-type cations at the vertices of the tetrahedron. For every coordination we consider the relationship between the A-C and B-C distances when an anion is displaced from its central position. We assume that the influence of disorder in the NNN and further shells does not affect the displacement of a central anion. The NNN interactions are much smaller than the NN ones but it is not necessary to assume that they are negligible. It is enough to observe that, due to the long-range disorder, the net displacing force acting on a central anion will be close to zero. Figure 12 shows all possible geometrical situations for the three cases in which we have 1, 2, or 3 B-type cations in a tetrahedron. We assume that the anion has a tendency to get closer to the B-type cation (in our case the B-type cation is Mn, in the case of Mikkelsen and Boyce[19] it is Ga).

If $z_n(x)$ denotes the B-C distances, the A-C distances are given by

$$y_1(x)=\left[\frac{a^2(x)}{2}+z_1^2(x)-\frac{2a(x)}{\sqrt{3}}z_1(x)\right]^{1/2},$$

$$y_2(x)=\left[\frac{a^2(x)}{4}-a(x)\left[z_2^2(x)-\frac{a^2(x)}{8}+z_2^2(x)\right]^{1/2}\right]^{1/2}, \tag{5}$$

$$y_3(x)=\frac{a(x)}{\sqrt{3}}-[4z_3^2(x)-\tfrac{2}{3}a^2(x)]^{1/2}/2,$$

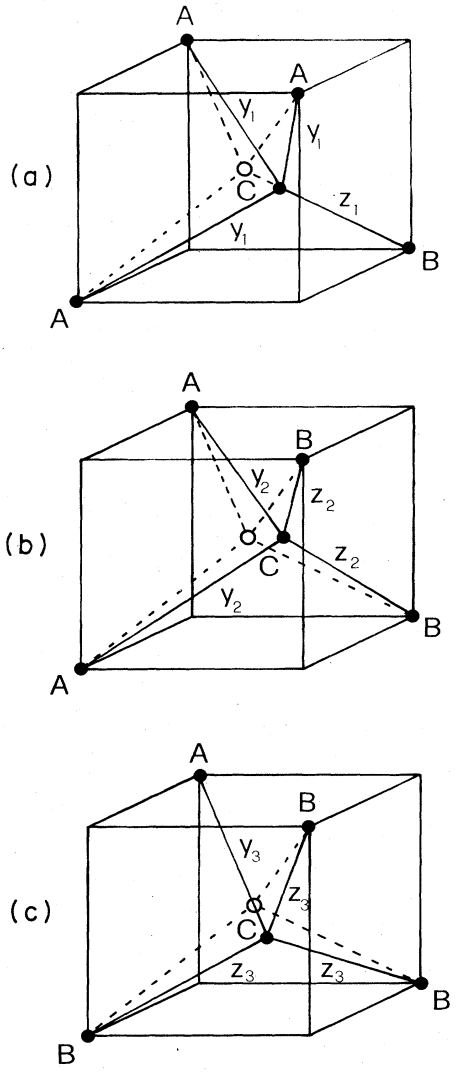

FIG. 12. All possible coordinations around the anion in the tetrahedra containing both types of cations. The open circle and dashed lines mark the positions of the central anion and the bonds in tetrahedra when the anion sublattice is undistorted. The solid lines and the solid circles mark the bonds and the positions of the ions in the distorted tetrahedra.

for the cases (a), (b), and (c) in Fig. 12, respectively; $a(x)$ denotes the lattice constant of the alloy at concentration x. In the case where all four cations are the same, the tetrahedron cannot be distorted—the B-C (or the A-C) distance equals $y_0=z_4=a(x)\sqrt{3}/4$.

(iii) In the next step we must consider the probability of finding tetrahedra with 0, 1, 2, 3, and 4 B-type cations in the alloy at concentration x. Let us assume, at the beginning, a random distribution of cations in their sublattice (possible deviations from full randomness will be discussed later). Obviously, the probability of finding the B-type cation at any vertex of the tetrahedron is equal to x and the probability of finding the A-type cation is $1-x$. Hence, the probability of finding a tetrahedron with n B-type cations is given by the binomial Bernoulli distribution:

$$P(n,x)=\begin{bmatrix}4\\n\end{bmatrix}x^n(1-x)^{4-n}\quad(n=0,1,3,4)\ . \tag{6}$$

Some remarks, concerning the model of Mikkelsen and Boyce,[19] are in order here. They claim that in the $A_{0.5}B_{0.5}C$ alloy the tetrahedra containing one and three, and three and one A-type and B-type cations, respectively, should occur 4.2 times less frequently than those with two A and two B cations. Their analogy to chalcopyrite is based on the observation that, in the $A_{0.5}B_{0.5}C$ alloy, tetrahedra with two A and two B cations are predominant. This is, unfortunately, not the case, because, in accordance with formula (6) for $x=0.5$, the probability of finding a tetrahedron with two A and two B cations is $\frac{3}{8}$, whereas those of 1-3 and 3-1 configurations are $\frac{1}{4}$ each. Hence, it is more likely that we will find a tetrahedron with a 1-3 or 3-1 configuration than one with a 2-2 configuration, even for $x=0.5$. It makes the validity of their chalcopyrite analogy questionable.

(iv) Having defined the geometry and the probability distribution of different possible tetrahedra, one can calculate the average NN distances. It can be done if the distances $y_n(x)$ and $z_n(x)$ are properly weighted by the probabilities (6) and the additional weights $W(n)=4-n$ [and $W(4-n)$] arising from the fact that in the tetrahedron containing n B-type cations there are $4-n$ A-C (and n B-C) distances. Then, the average A-C and B-C distances denoted by $\bar{y}$ and $\bar{z}$, respectively, are given by

$$\bar{y}(x)=\frac{1}{P(x)}\sum_{n=0}^{4}W(n)P(n,x)y_n(x)\ , \tag{7}$$

where

$$P(x)=\sum_{n=0}^{4}W(n)P(n,x)$$

and

$$\bar{z}(x)=\frac{1}{P'(x)}\sum_{n=0}^{4}W(4-n)P(n,x)z_n(x)\ , \tag{8}$$

where

$$P'(x)=\sum_{n=0}^{4}W(4-n)P(n,x)\ .$$

(v) To complete the calculation of the average NN distances, we need to know all six values $y_n(x)$,$z_n(x)$ $(n=1,2,3)$, and to realize this, the following procedure is proposed. The $\eta_n(x)$, given below, are minimized with respect to $z_n(x)$ for all cases $n=1,2,3$, and for each value of x,

$$\eta_n(x)=\frac{3\alpha_z}{8z_p^2}W(4-n)[z_n^2(x)-z_p^2]^2+\frac{3\alpha_y}{8y_p^2}W(n)[y_n^2(x)-y_p^2]^2\ . \tag{9}$$

The z_p and y_p denote the B-C and A-C NN distances in the pure BC and AC compounds, and α_z and α_y denote the bond-stretching constants of these compounds, respectively. The functions (9) can be interpreted as the energies

needed for changing the bond lengths and they are written on the basis of Keating's[31] scheme of the valence-force-field (VFF) approach.[32] The bond-stretching constants are taken from the paper by Martin,[33] and bond-bending terms are neglected. The fact that the minimization is carried out for each configuration of atoms in each tetrahedron is consistent with the assumption of the dominant role of the NN interactions. Furthermore, it should be noted that the proposed minimization procedure follows the empirical observation, mentioned above, that the A-C and B-C distances in the $A_{1-x}B_xC$ alloy tend to be, as far as possible, the same as those in the pure compounds.

In order to check the validity of our assumptions, we have also minimized $\eta_n(x)$ with the bond-bending terms and a relaxed cation sublattice. We have found that for both $Cd_{1-x}Mn_xTe$ and $In_{1-x}Ga_xAs$ the average NN bond lengths are slightly (0.1%) modified.[34] If one adds the bond-bending terms in Eq. (9) and does not allow for any relaxation of the cations, or if one relaxes the cations and does not include the bond-bending terms, large errors in the average distances will be found. In view of these results we are justified in adopting the present model as a reasonable approximation.

Steps (i)—(v) form a complete model of an alloy. The procedure can be summarized in a few words: The set of values $z_n(x)$ and $y_n(x)$ has been obtained by means of the minimization of functions (9) with the use of relations (5); from Eqs. (7) and (8) $\bar{z}(x)$ and $\bar{y}(x)$, the average NN distances were calculated. The sufficient input data for the calculation are the lattice constants of the alloy $a(x)$ and the bond-stretching constants of the components. Obviously, $z_p = a(1)\sqrt{3}/4$ and $y_p = a(0)\sqrt{3}/4$.

B. Application to $Cd_{1-x}Mn_xTe$ and $In_{1-x}Ga_xAs$ alloys

The lattice constants for CdTe [$a(0)=6.468$ Å] and $Cd_{1-x}Mn_xTe$ ($0 \leq x \leq 0.7$) were obtained from the x-ray diffraction data.[18] The linear dependence of $a(x)$ was extrapolated and the value $a(1)=6.333$ Å for pure MnTe was obtained. The bond-stretching constants, as mentioned above, were taken from the literature.[33] For CdTe, $\alpha_{CdTe}=29.02$, and for MnTe the value $\alpha_{ZnTe}=31.35$ was used as an approximation. This is perhaps not very well justified, but one should note that the values of the force constants are not critical. The equilibrium positions calculated by minimizing η are only weakly dependent on these values. In the particular cases where η reaches its absolute minimum equal to 0, the equilibrium position does not depend on α at all. Most of the effective physical interactions are built in the model via the undistorted bond lengths z_p and y_p.

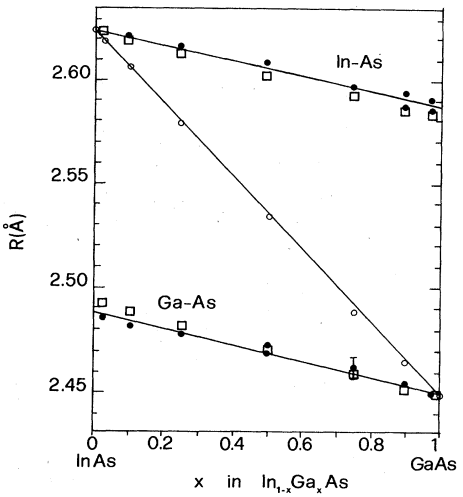

FIG. 13. Average In-As and Ga-As nearest-neighbor distances in $In_{1-x}Ga_xAs$ alloys vs concentration x. All symbols and lines are as in Fig. 11.

The results of the calculations for $Cd_{1-x}Mn_xTe$ are illustrated in Fig. 11 and detailed values are presented in Table II. Figure 13 and Table III show the results of the application of our model to the data of Mikkelsen and Boyce.[19] The bond-stretching constants of InAs and GaAs were also taken from the literature.[33] The rms deviation σ of the NN distributions calculated for both the In-As and the Ga-As distances are included in Table III. In both cases the agreement is rather good, although the calculated straight lines possess slightly greater slope than the experimental ones and the broadening of the NN distance distribution suggested by our model is a little larger than that observed.[19] However, since our model is based on the assumption that the cation sublattice remains fixed, it does not reproduce the different NNN distances in the cation sublattice of $In_{1-x}Ga_xAs$ (Ref. 19, Fig. 9).

C. Additional comments on the model

Finally, we would like to add the following remarks:
(i) It is possible to relax the first assumption of our

TABLE II. NN distances in the $Cd_{1-x}Mn_xTe$ alloy vs concentration x. The values y_1,y_2,y_3 and z_1,z_2,z_3 are the distances obtained for different configurations (a), (b), and (c) in Fig. 12, respectively. $\bar{y}$ and $\bar{z}$ are the NN average distances. $a(x)$ is the lattice constant and $y_0(z_4)$ is the NN distance in the undistorted tetrahedron. All distances are in Å.

		Cd-Te distance					Mn-Te distance			
x	$a(x)$	$\bar{y}$	y_1	y_2	y_3	$y_0(z_4)$	z_1	z_2	z_3	$\bar{z}$
0.1	6.455	2.800	2.810	2.825	2.840	2.795	2.751	2.766	2.780	2.755
0.3	6.428	2.797	2.798	2.813	2.828	2.783	2.739	2.754	2.769	2.753
0.5	6.401	2.794	2.786	2.801	2.816	2.772	2.728	2.742	2.757	2.750
0.7	6.373	2.791	2.774	2.782	2.804	2.760	2.716	2.731	2.745	2.748

TABLE III. NN distances and rms deviations $\sigma_y(\overline{y^2}-\overline{y}^2)^{1/2}$ and $\sigma_z=(\overline{z^2}-\overline{z}^2)^{1/2}$ for $In_{1-x}Ga_xAs$ as a function of the concentration x. All symbols as in Table II.

In-As distance							
x	$a(x)$	$\overline{y}$	y_1	y_2	y_3	σ_y	$y_0(z_4)$
0.025	6.045	2.621	2.664	2.709	2.751	0.012	2.618
0.1	6.015	2.618	2.650	2.695	2.738	0.024	2.605
0.25	5.955	2.613	2.624	2.669	2.712	0.034	2.578
0.5	5.854	2.602	2.580	2.625	2.668	0.038	2.535
0.75	5.754	2.592	2.536	2.581	2.624	0.033	2.491
0.9	5.694	2.585	2.510	2.555	2.599	0.023	2.465
0.099	5.657	2.582	2.494	2.539	2.583	0.008	2.450

Ga-As distance						
x	$a(x)$	z_1	z_2	z_3	$\overline{z}$	σ_z
0.025	6.045	2.488	2.533	2.576	2.492	0.012
0.1	6.015	2.475	2.520	2.563	2.489	0.023
0.25	5.955	2.450	2.494	2.537	2.483	0.033
0.5	5.854	2.408	2.451	2.494	2.472	0.036
0.75	5.754	2.365	2.408	2.450	2.460	0.031
0.9	5.694	2.339	2.382	2.424	2.453	0.021
0.099	5.657	2.324	2.366	2.409	2.449	0.007

model and let the cations move a little away from the vertices of the tetrahedron. Then the displacements of the ions in both sublattices should be calculated in a self-consistent way. Unfortunately, this will change our simple model to a very complex one. The bond-bending terms in the full Keating scheme should also be included.

(ii) In some other applications not only the average values $\overline{z}$ and $\overline{y}$ but the NN distances z_n and y_n (as listed in Tables II and III) may be useful as well.

(iii) The expression for the average over *all* NN distances can be written in two equivalent forms [see Eqs. (7) and (8)]:

$$D=\frac{1}{P(x)+P'(x)}\left[\sum_{n=0}^{4}W(n)P(n,x)y_n(x)+\sum_{n=0}^{4}W(4-n)P(n,x)z_n(x)\right] \quad (10)$$

or

$$D=(1-x)\overline{y}(x)+x\overline{z}(x)\ . \quad (11)$$

The latter was proposed by Mikkelsen and Boyce.[19] Comparing Eq. (11) with Eq. (10) one can thus understand the internal structure of the phenomenological expression (11). If we evaluate the expression (10) using all NN distances as listed in Tables II and III, we will obtain the average NN distance D as measured by x-ray diffraction in the particular cases. Such a test of consistency was done, showing perfect agreement.

(iv) A general structure of the model is one in which the average positions of the anions in the distorted sublattice are at the center of the tetrahedron, independently of the assumption of a random distribution. This means that the average over *all* possible NNN distances between anions will not differ from the value of the NNN distance in an undistorted sublattice or, in other words, from the VCA value. In spite of that, the distribution of the NNN distances between anions will show a multimodal character similar to that of the NN distances. We have derived the NNN distribution for both alloys with a Monte Carlo calculation using five coordination shells of neighbors around the central anion. The cation sublattice is occupied randomly and the anions are put in the positions specified in Tables II and III. Figure 14 shows the results for $In_{1-x}Ga_xAs$ for $x=0.25$, 0.5, and 0.75. The results for $Cd_{1-x}Mn_xTe$ are qualitatively similar. To help the comparison with the experimental data,[19] we have convoluted each histogram with a Gaussian distribution. Particularly interesting is the case $x=0.5$ because it can be directly compared with the pseudochalcopyrite model of Mikkelsen and Boyce.[19] This distribution consists of three main distances at 4.04, 4.12, and 4.24 Å, to be compared with the measured EXAFS values 4.02, 4.26 Å. For the pseudochalcopyrite structure (top panel of Fig. 14) the Monte Carlo distribution peaks approximately at 4.04 and 4.20 Å, in agreement with the averaged distances reported in Ref. 19. For $x=0.5$ we have, however, the group of distances at 4.14 Å, the distance between anions in the undistorted sublattice. Such a distance occurs when two anions in adjacent tetrahedra have identical environments. Closer analysis reveals that such a situation can

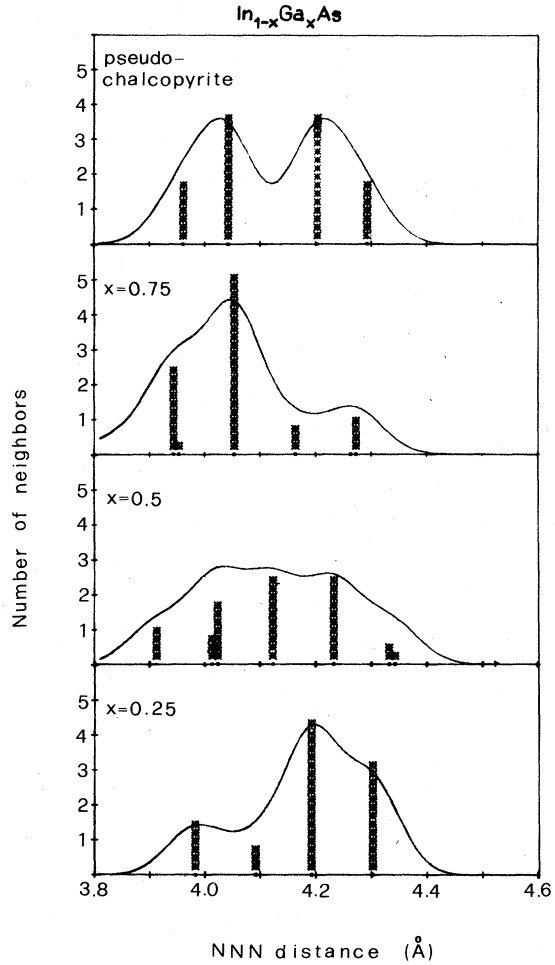

FIG. 14. Second-nearest-neighbor distributions for $In_{1-x}Ga_xAs$. Histogram-bar widths are equal to 0.01 Å. The highest histogram shows the distribution for the pseudochalcopyrite model. The solid curves are the convolution of the histograms with a Gaussian distribution ($\sigma^2=0.0025$ Å^2).

occur in two distinct cases: First, two adjacent tetrahedra contain only type-A or type-B cations (the anions are not displaced from their zinc-blende sites); second, two 2×2 tetrahedra are adjacent and identically oriented in space (the anions are displaced coherently and the distance between them does not change). For 3×1 and 1×3 tetrahedra such a situation is excluded. The first case does not contribute much to the distribution at 4.14 Å ($<1\%$) on account of the low probability of finding two adjacent tetrahedra with only A (B) -type cations. If the cation sublattice is randomly occupied, the second case occurs frequently; it is, however, interesting to note that in the chalcopyrite structure it never occurs. The data of Mikkelsen and Boyce[19] suggest that it occurs less frequently for the $x=0.5$ alloy. It is, however, to be noted that this fact can be to some extent reconciled with our model. Suppose that for some reasons (essentially the same which make the chalcopyrite structure stable) when two 2×2 tetrahedra are adjacent they are preferably oriented in a different way in space (intertetrahedra correlation). In such a case the presence of the 4.14 Å distance will be absent in the NNN distribution. One should, however, realize that introducing *ad hoc* intertetrahedra correlations cannot be reconciled with the assumption of a perfectly random distribution of cations in their sublattice. The presence of the central peak for $x=0.5$ is the main discrepancy between our model and the experiment. The assumption about such an intertetrahedra correlation is weakly substantiated,[34] although it remains in agreement with the chalcopyrite analogy of Mikkelsen and Boyce. The problem remains open, but we want to mention that from the results of the generalized model[35] in which the cation sublattice is allowed to relax and the bond-bending terms are included, the central peak remains as well.

(v) The ultimate minimum of η is obviously equal to 0 and can occur when $z_n(x)=z_p$ and $y_n(x)=y_p$. It will be interesting to see if and when such a situation can take place. η depends on x only via the lattice constant $a(x)$. If we assume a linear dependence of the lattice constant on the composition, i.e., $a(x)=mx+b$, we easily find that η_n is equal to 0 for x almost equal to 0.25, 0.5, and 0.75 for $n=1$, 2, and 3, respectively (actual values for $Cd_{1-x}Mn_xTe$ are 0.254, 0.505, and 0.754, and, for $In_{1-x}Ga_xAs$, 0.262, 0.517, and 0.764). Physically, it means that, for these particular concentrations in the tetrahedra of types 1, 2, and 3, respectively, the bond lengths can be exactly the same as those in the pure compounds. At the same time, the probability of finding such a tetrahedron is the highest one. One can, therefore, intuitively see that the linear behavior of $a(x)$ is connected with the energy minimization in the alloy. One should note, moreover, that formula (9), obtained on the basis of a linear dependence of the lattice constant on composition, is just equivalent to a "tetrahedral bond conservation rule," the old idea of Bragg, discussed extensively in a recent paper by Jaffe and Zunger.[36] They argue that for the chalcopyrite materials the bond length can be fitted simply by a sum of atomic radii, and that the A-C bond length does not depend on the B atom. Formula (9) extends this idea to the $1A$-$3B$ and the $3A$-$1B$ tetrahedra as well. On the basis of the above considerations, we can calculate the value of 1.42 Å as a tetrahedral ionic radius for Mn^{2+} (Ref. 37).

(vi) Our model does not consider the problem of the violation of the random distribution of cations in the alloy. All quantitative results and conclusions drawn from it when confronted with experimental data of different measurements (x-ray diffraction, EXAFS, magnetic) may or may not confirm such a violation. However, there is explicit evidence that for the diluted $In_{1-x}Ga_xAs$ alloy the distribution of the cations is random and the deviation from randomness is estimated to be not larger than 15% for concentrated alloys.[19] Support against chemical clustering of Mn ions may be drawn from EXAFS studies of other magnetic alloys.[38]

In the limited framework of our model we cannot answer this important question definitely. The agreement of the calculated and measured average NN distances suggests the absence of a strong clustering. One can argue that it is possible, in general, to obtain the same average values using different distributions; here, however, we

reproduce the experimental curves rather than just single points, using the same distribution. The lines describing the dependence of NN distances on x have slopes different from 0; it is apparent especially for $In_{1-x}Ga_xAs$. If the clustering is significant and if the tetrahedral bond-conservation rule holds, these lines should be parallel to the x axis. Since, however, the experimental evidence is in favor of a random distribution, one should answer the question of why the tetrahedra for which the η values are the lowest do not predominate? The calculated values of η are of the order of 20 meV ($\sim$250 K) for $Cd_{1-x}Mn_xTe$ and 100 meV ($\sim$1200 K) for $In_{1-x}Ga_xAs$. The alloy-formation temperatures are well above 1000 K in both cases. The thermal energy is evidently high enough to make all the configurations equally probable as far as thermodynamics is concerned. When the temperature decreases, the configurations remain frozen, although for $Cd_{1-x}Mn_xTe$ even this assumption is not necessary. Hence, we conclude that the random distribution of different cations in the cation sublattice is almost perfect in $Cd_{1-x}Mn_xTe$. For $In_{1-x}Ga_xAs$ a clustering process in the limit mentioned above is possible. A deeper thermodynamical study of the problem is, however, highly desirable.

IV. DISCUSSION AND CONCLUSIONS

The EXAFS studies of the Te, Cd, and Mn edges in $Cd_{1-x}Mn_xTe$ alloys bring the following significant conclusions:

(i) At the L_{III} edge of Te (Fig. 10), the NN peak is split into two peaks. The simulation confirms that they are related to Mn and Cd backscatterers at two different distances, 2.74–2.755 Å (depending on x) and 2.80 Å, from the Te absorber, respectively. In $Cd_{1-x}Mn_xTe$ the modulus $F(R)$ of the separated Cd and Mn peaks significantly decreases and increases with increasing Mn content, respectively.

(ii) In CdTe at the L_{III} edge of Te, the peak at about 4.3 Å is composed of unresolved peaks due to the Te second shell and the third shell of Cd. In the $Cd_{1-x}Mn_xTe$ alloy the position of this complex peak does not change appreciably with x.

(iii) Within the experimental resolution the position and the width of the Te peaks at the Cd L_{III} edge are approximately the same for various concentrations of Mn. As described in Sec. II C, the Te-Cd average distance equals 2.80 ± 0.01 Å and it is almost independent of x.

(iv) From the Mn K–edge data, the Te-Mn average distance changes from 2.76 to 2.74 Å with increasing x. Also, the overall width of the Te peak is approximately the same for various concentrations of Mn.

We would like to emphasize that the NN distances obtained from Cd L_{III} and Mn K edges are in agreement with those obtained from the Te L_{III} edge. These results are direct experimental evidence confirming the bimodal distribution of the NN distances in $Cd_{1-x}Mn_xTe$ alloys, which demonstrates the existence of two different, well-defined average distances between Te-Cd and Te-Mn.

The model of the microscopic structure of the zinc-blende-type $A_{1-x}B_xC$ alloys gives all the particular NN distances as well as the average NN distances, in good quantitative agreement with both our experimental data and that of Mikkelsen and Boyce.[19] The analysis of the model enables us also to understand the behavior of NNN distances as described in Ref. 19 (our experimental resolution was insufficient to observe such subtle changes in $Cd_{1-x}Mn_xTe$).

We believe that the local distortion in zinc-blende-type $A_{1-x}B_xC$ alloys described by our model is a *universal* feature of such alloys. One of the important consequences is that it makes the "classical" definition of the VCA questionable. One either must accept that the VCA is not really a very good model because in this approximation all distortions of the sublattices are ignored, or one must consider the generalization of the VCA which also includes a proper averaging of the potential of C atoms over *all* possible positions in their distorted sublattice.

The same can be applied to more sophisticated one-electron alloy theories such as the coherent-potential approximation (CPA) or average–t-matrix approximation (ATA).[39] Besides taking into account the scattering on the different cations, one should also incorporate into these theories in some way the effects of averaging the anion potential over different geometrical sites.

Finally, we would like to discuss the problem of the stability of the tetrahedral coordination in $Cd_{1-x}Mn_xTe$ alloys. According to the approach of Phillips and Van Vechten,[39] the ionicity of CdTe is equal to 0.717, which is close to the critical ionicity value (0.785) at which the transition from a covalent to an ionic structure or, in other words, the transition from the fourfold (zinc-blende, wurtzite) to the sixfold (rocksalt, NiAs) coordination occurs. Since Mn in MnTe has sixfold coordination, MnTe is reported to be more ionic than CdTe.[37] This indication is supported by core-level shifts from x-ray photoemission spectra[41] and effective charge calculations.[42] The addition of Mn in CdTe should increase the ionicity of the bonds. The question arises as to how the crystal structure of $Cd_{1-x}Mn_xTe$ can still be cubic up to $x=0.7$, taking into account that CdTe is already close to the structural phase transition. The answer is that the local distortions of the lattice (distortions of the tetrahedra) described by our model stabilize the zinc-blende-type structure up to $x=0.7$. To understand this point one should note the following:

(i) In nearly covalent compounds the center of gravity of the bonding charge is placed almost at the middle of the bond, and shifts towards an anion when the bond ionicity increases.

(ii) The distortion of the tetrahedra containing 1, 2, or 3 Mn ions, i.e., the shift of the Te ions towards Mn compensates for the displacement of the center of gravity of the bonding charge and decreases the effective bond ionicity. Such a shift is also favored by the smaller ionic radius of Mn^{2+} ions compared to that of Cd^{2+}.

(iii) The probability of finding a tetrahedron with four Mn ions increases rapidly for $x>0.7$ [see formula (6)]. Such tetrahedra, according to our model, cannot be distorted and the displacement of the bonding charge cannot be compensated. Therefore, the fourfold coordination of $Cd_{1-x}Mn_xTe$ becomes unstable and the transition to a

phase typical for ionic compounds occurs.

Summarizing the discussion about the stability of the $Cd_{1-x}Mn_xTe$ alloys, we would like to say that phenomenological considerations about ionicity, supported by conclusions drawn from our theoretical model of the microscopic structure, gives a satisfactory, qualitative explanation of this problem.

ACKNOWLEDGMENTS

We would like to thank Professor W. Giriat, Dr. S. A. Ignatowicz, and Mr. H. Weiers for supplying the samples. We also thank Dr. J. Soltys for the x-ray diffraction analysis and Dr. S. Mobilio for providing part of the fitting program used here. We thank the Programma per l'Utilizzazione della Luce di Sincrotrone (PULS) group of the Laboratori Nasionali di Frascati, Istituto Nazionale di Fisica Nucleare, for their hospitality. Four of us (A.K., M.P., M.Z.-S., and M.T.-C.) also acknowledge the Universities of Rome I and Rome II for financial support. M.P. wishes to acknowledge financial support obtained from the Alexander von Humboldt Foundation. This work was supported in part by the Italian Gruppo Nazionale di Struttura della Materia, Consiglio Nazionale delle Ricerche (GNSM) through the Ministero della Pubblica Istruzione.

*On leave of absence from the Institute of Physics of the Jagiellonian University, PL-30-059 Cracow, Poland.

[1]N. T. Khoi and J. A. Gaj, Phys. Status Solidi B **83**, K133 (1977).

[2]J. Stankiewicz, N. Bottka, and W. Giriat, in Proceedings of the 15th International Conference on the Physics of Semiconductors, Kyoto [J. Phys. Soc. Jpn. Suppl. A **49**, 827 (1980)].

[3]R. A. Abreu, W. Giriat, and M. P. Vecchi, Phys. Lett. **85A**, 399 (1981).

[4]J. Diouri, J. P. Lascaray, and R. Triboulet, Solid State Commun. **42**, 231 (1982).

[5]J. A. Gaj, R. R. Gałazka, and M. Nawrocki, Solid State Commun. **25**, 193 (1978).

[6]J. A. Gaj, J. Ginter, and R. R. Gałazka, Phys. Status Solidi B **89**, 655 (1978).

[7]G. Rebmann, C. Rigaux, G. Bastard, M. Menant, R. Triboulet, W. Giriat, in Proceedings of the 16th International Conference on the Physics of Semiconductors, Montpellier (1982) [Physica **117&118B+C** (1983)].

[8]J. Stankiewicz and A. Aray, J. Appl. Phys. **53**, 3117 (1982).

[9]S. B. Oseroff, R. Calvo, W. Giriat, and Z. Fisk, Solid State Commun. **35**, 559 (1980).

[10]R. R. Gałazka, S. Nagata, and P. M. Keesom, Phys. Rev. B **22**, 3344 (1980).

[11]H. Kett, W. Gebhart, V. Krey, and J. K. Furdyna, J. Magn. Magn. Mater. **25**, 215 (1981).

[12]M. Escorne and A. Mauger, Phys. Rev. B **25**, 4674 (1982).

[13]M. P. Vecchi, W. Giriat, and L. Videla, Appl. Phys. Lett. **38**, 99 (1981).

[14]B. A. Orłowski, Phys. Status Solidi B **95**, K31 (1979); C. Webb, M. Kaminska, M. Lichtensteiger, and J. Lagowski, Solidi State Commun. **40**, 609 (1981).

[15]P. Oelhafen, M. P. Vecchi, J. L. Freeouf, and V. L. Moruzzi, Solid State Commun. **44**, 1547 (1982).

[16]R. R. Gałazka, in *Physics of Semiconductors 1978*, edited by B. L. H. Wilson (The Institute of Physics, Bristol, England, 1979), p. 133.

[17]S. Venengopalau, A. Petrou, R. R. Gałazka, and A. K. Radamas, Solid State Commun. **35**, 401 (1980).

[18]M. Zimnal-Starnawska, Ph.D. thesis, Jagiellonian University, 1980 (unpublished).

[19]J. C. Mikkelsen and J. B. Boyce, Phys. Rev. Lett. **49**, 1412 (1982); Phys. Rev. B **28**, 7130 (1983).

[20]J. Azoulay, E. A. Stern, D. Shalteil, and A. Grayewski, Phys. Rev. B **25**, 5627 (1982).

[21]F. Antonangeli, A. Balzarotti, N. Motta, M. Piacentini, A. Kisiel, M. Zimnal-Starnawska, and W. Giriat, in *EXAFS and Near Edge Structure*, edited by A. Bianconi, L. Incoccia, and S. Stipcich (Springer, Berlin, 1983), p. 224.

[22]A. Balzarotti, M. T. Czyzyk, A. Kisiel, N. Motta, M. Podgorny, and M. Zimnal-Starnawska, Phys. Rev. B **30**, 2295 (1984); A. Balzarotti, A. Kisiel, N. Motta, M. Zimnal-Starnawska, M. T. Czyzyk, and M. Podgorny, in *Progress in Crystal Growth and Characterization*, edited by R. Pamplin (Pergamon, Oxford, 1985), Vol. 10, p. 55.

[23]T. Kendelewicz, Solid State Commun. **36**, 127 (1980).

[24]M. Zimnal-Starnawska, M. Podgorny, A. Kisiel, W. Giriat, W. Demianiuk, and J. Zmija, J. Phys. C **17**, 615 (1984).

[25]M. T. Czyzyk and M. Podgorny, in *Proceedings of the Conference on the Physics of Semiconductor Compounds, Jaszowiec, 1983* (Ossolineum, Warsaw, 1984), Vol. 5.

[26]A. Balzarotti, M. De Crescenzi, and L. Incoccia, Phys. Rev. B **25**, 6349 (1982); S. Mobilio, F. Comin, and L. Incoccia, Frascati Laboratories Internal Report LNF-82/19-(NT) (unpublished).

[27]P. A. Lee, P. H. Citrin, P. Eisemberger, and B. M. Kincaid, Rev. Mod. Phys. **53**, 769 (1981); T. M. Hayes and J. B. Boyce, in *Solid State Physics*, edited by F. Seitz, D. Turnbull, and H. Ehrenreich (Academic, New York, 1982), Vol. 37, p. 173.

[28]B. K. Teo and P. A. Lee, J. Am. Chem. Soc. **101**, 2815 (1979).

[29]E. A. Stern, B. A. Bunker, and S. M. Heald, Phys. Rev. B **21**, 5521 (1980).

[30]R. F. Pettifer, in *Inner-Shell and X-Ray Physics of Atoms and Solids*, edited by D. J. Fabian, H. Kleinpoppen, and L. M. Watson (Plenum, New York, 1980).

[31]P. N. Keating, Phys. Rev. **145**, 637 (1966).

[32]M. J. P. Musgrave and J. A. Pople, Proc. R. Soc. London, Ser. A **268**, 474 (1962).

[33]R. M. Martin, Phys. Rev. B **1**, 4005 (1970).

[34]N. Motta, A. Balzarotti, P. Letardi, A. Kisiel, M. T. Czyzyk, M. Zimnal-Starnawska, and M. Podgorny, Solid State Commun. **53**, 509 (1985).

[35]An approach including both these extensions will be presented in a separate paper.

[36]A. Zunger and J. E. Jaffe, Phys. Rev. Lett. **51**, 662 (1983); J. E. Jaffe and A. Zunger, Phys. Rev. B **29**, 1882 (1984).

[37]L. Pauling, *The Nature of the Chemical Bond* (Cornell University Press, New York, 1960).

[38]T. M. Hayes, J. W. Allen, J. B. Boyce, and J. J. Hauser, Phys. Rev. B **22**, 4503 (1980).

[39]See, e.g., D. J. Sellmyer, in *Solid State Physics,* edited by F. Seitz, D. Turnbull, and H. Ehrenreich (Academic, New York, 1978), Vol. 33, p. 83.

[40]J. C. Phillips, *Bond and Bands in Semiconductors* (Academic, New York, 1973), and references therein.

[41]H. Franzen and C. Sterner, J. Solid State Chem. **25**, 227 (1978).

[42]J. W. Allen, G. Lucovsky, and J. C. Mikkelsen, Jr., Solid State Commun. **24**, 367 (1977).